Energy level decay and excited state absorption processes in erbium-doped tellurite glass

Laércio Gomes,[1] Michael Oermann,[2] Heike Ebendorff-Heidepriem,[2] David Ottaway,[2] Tanya Monro,[2] André Felipe Henriques Librantz,[3] and Stuart D. Jackson[4,a)]
[1]*Center for Lasers and Applications, IPEN/CNEN-SP, P.O. Box 11049, São Paulo, SP 05422-970, Brazil*
[2]*Physics Building, North Terrace Campus, Institute for Photonics & Advanced Sensing, The University of Adelaide, SA 5005 Australia*
[3]*Center for Lasers and Applications, IPEN/CNEN-SP, P.O. Box 11049, São Paulo, SP 05422-970, Brazil and Sciences Department, UNINOVE, São Paulo, SP 01156-050, Brazil*
[4]*School of Physics, Institute of Photonics and Optical Science, University of Sydney, Camperdown 2006 Australia*

(Received 21 June 2011; accepted 7 September 2011; published online 25 October 2011)

The fundamental excited state decay processes relating to the $^4I_{11/2} \rightarrow {}^4I_{13/2}$ transition in singly Er^{3+}-doped tellurite (TZNL) glass have been investigated in detail using time-resolved fluorescence spectroscopy. Selective laser excitation of the $^4I_{11/2}$ energy level at 970 nm and selective laser excitation of the $^4I_{13/2}$ energy level at 1485 nm has established that energy transfer upconversion by way of a dipole-dipole interaction between two excited erbium ions in the $^4I_{13/2}$ level populates the $^4I_{11/2}$ upper laser level of the 3 μm transition. This upconversion has been analyzed for Er_2O_3 concentrations between 0.5 mol. % and 2.2 mol. %. The $^4I_{13/2}$ and $^4I_{11/2}$ energy levels emit luminescence with peaks located at 1532 nm and 2734 nm, respectively, with radiative decay efficiencies of 65% and 6.8% for the higher (2.2 mol. %) concentration sample. The low 2.7 μm emission efficiency is due to the non-radiative decay bridging the $^4I_{11/2} \rightarrow {}^4I_{13/2}$ transition and energy transfer to the OH^- groups in the glass. Excited state absorption was observed to occur from the $^4I_{13/2}$ and $^4I_{11/2}$ levels with peak absorptions occurring at 1550 nm and 971 nm, respectively. The decay time of the $^4I_{11/2}$ excited state decreased with an increase in the Er^{3+} concentration, which related to energy transfer to OH^- ions that had a measured concentration of 6.6×10^{18} cm^{-3}. Results from numerical simulations showed that a population inversion is reached at a threshold pumping intensity of $\sim$80 kW cm^{-2} for a cw laser pump at 976 nm if $[Er^{3+}] \geq 1.2 \times 10^{21}$ cm^{-3} (or $[Er_2O_3] \geq 2.65$ mol. %) without OH^- impurities being present. © *2011 American Institute of Physics*. [doi:10.1063/1.3651399]

I. INTRODUCTION

The strong interest in the generation of light at mid-infrared wavelengths (between 3 μm and 50 μm) is being driven by applications in medicine, defence, and spectroscopy. With the field of mid-infrared photonics growing fast, the search for stable efficient and cost effective sources of light at wavelengths approaching 3 μm is strong. The majority of mid-infrared laser research has concentrated on a number of rare earth ions when they are doped into low phonon energy crystals such as $LaCl_3$ (Ref. 1) and KPb_2Cl_5 (Ref. 2) and low phonon energy glasses e.g., the chalcogenides.[3,4] Stability issues are a hindrance for these materials and for the generation of high power, a long gain medium length and large mode area can be achieved through the use of a fiber geometry.

The use of the fiber geometry for the generation of mid-infrared laser radiation provides good thermal management and a comparatively lower threshold because of the extended longitudinal dimension and small transverse cross section relevant to optical fibers. The $^4I_{11/2} \rightarrow {}^4I_{13/2}$ transition of Er^{3+} is a four level laser transition that offers broadband fluorescence in the 3 μm wavelength range. To date, high power fibre lasers emitting on this transition have been achieved only in fluorozirconate based fibres.[5–8] Due to the hygroscopic nature of fluoride based glasses, it is difficult to avoid the degradation of the glass that occurs when exposed to moisture in the atmosphere. Tellurite glasses show potential as an alternative oxide based host material due to their relatively low maximum phonon energies ($\sim$690 cm^{-1} for the Er^{3+}-doped tellurite (TZNL) glass composition used here) when compared to other oxide glasses.[9] They also have good transmission between 0.35 and 5 μm and are less susceptible to the crystallization and degradation that can occur in fluoride glasses.[9] To further explore the potential of the $^4I_{11/2} \rightarrow {}^4I_{15/2}$ transition in tellurite glass and to offer the possibility of highly efficient Er^{3+} laser operating at 3 μm in an oxide based glass, detailed spectroscopic studies are required. These studies would reveal the important energy transfer and energy level decay processes that relate to the $^4I_{11/2} \rightarrow {}^4I_{13/2}$ transition in tellurite glass.

To fulfill this objective, we have prepared a number of Er_2O_3-doped tellurite glasses of varying Er_2O_3 concentration (0.5 to 2.2 mol. %) and measured the luminescence decay characteristics after selective energy level excitation. The luminescence efficiencies of these levels were determined when the experimental decay time was compared with the

a)Author to whom correspondence should be addressed. Electronic mail: s.jackson@usyd.edu.au.

radiative lifetimes calculated using Judd-Ofelt theory. Due to the high O-H phonon energy, the cross-relaxation (CR) and energy transfer to OH^- impurities in the host glass result in the depopulation of the $^4I_{11/2}$ and $^4I_{13/2}$ energy levels and the rapid decay of the excited ions back to the ground state. The energy transfer rates to the OH^- groups in the glass are measured for these energy levels. Measurements of the pump excited state absorption (ESA), energy transfer upconversion (ETU), and CR parameters have also been obtained.

II. EXPERIMENTAL PROCEDURE

The TZNL (Ref. 10) glass samples used for the time-resolved luminescence spectroscopy were prepared from high purity raw materials with 99.99% pure TeO_2, ZnO and La_2O_3 and 99.999% pure Na_2CO_3 and had the composition: 73.3 TeO_2 + 19.6 ZnO + 4.9 Na_2O + (2.2- x) La_2O_3 + x Er_2O_3 with $x = 0.5$, 1.1, 2.2 mol. %. The starting powder materials were melted in a Pt-Au crucible in a dry glovebox environment, reducing the OH content in the glass, at 900 °C for 30 min. The liquids were poured into polished brass molds and annealed at 315 °C for 4 h to remove any mechanical stresses. The samples were then cut and polished into $8 \times 10 \times 12$ mm^3 rectangular prisms. The Er^{3+} ion densities were calculated to be 2×10^{20} cm^{-3}, 5×10^{20} cm^{-3}, and 1×10^{21} cm^{-3} for the doped tellurite samples with 0.5, 1.1, and 2.2 mol. % Er_2O_3, respectively.

Absorption spectra in the range of 2000–10 000 nm were measured using a FTIR spectrophotometer (Nicolet 6700). The decay characteristics of the excited states of Er^{3+} were measured using pulsed 12 mJ (4 ns, 10 Hz) laser excitation from a tunable optical parametric oscillator (OPO) pumped by the second harmonic of a Q-switched Nd-YAG laser (Brilliant B from Quantel). Tunable laser excitation from the OPO was used to excite the $^4I_{11/2}$ energy levels at 970 nm and $^4I_{13/2}$ energy levels at 1485 nm energy levels directly. The infrared luminescence (for $\lambda > 1080$ nm) was detected using an InSb infrared detector (Judson model J-10 D cooled to 77 K) in conjunction with a fast preamplifier with a response time of ~0.5 μs and analyzed using a digital 200 MHz oscilloscope (Tektronix TDS 410). The visible and near infrared ($\lambda < 1100$ nm) was detected using a photomultiplier tube (EMI) with a sensitive cathode of S-1 or S-2 type (PMT EMI refrigerated at –20 °C) with a response time of 20 ns. All the fluorescence decay characteristics were measured at 300 K. To isolate the infrared luminescence signals, bandpass filters each with ~80% transmission at 1500 nm or 2750 nm with a half width of 25 nm and an extinction coefficient of $\sim 10^{-5}$ outside this band were used.

III. EXPERIMENTAL RESULTS

The optical absorption spectrum of Er^{3+} ions in tellurite glass has two peak absorptions in the near infrared, one at approximately 1550 nm and the second near 980 nm. When the Er^{3+}-doped material is excited at 970 nm, the following processes are observed to occur:

(*a*) Ground state absorption (GSA)

$$Er^{3+}(^4I_{15/2}) + h\nu\ (980\,nm) \rightarrow Er^{3+}(^4I_{11/2})$$

(*a'*) ESA

$$Er^{3+}(^4I_{11/2}) + h\nu\ (980\,nm) \rightarrow Er^{3+}(^4F_{7/2}) \rightarrow Er^{3+}(^4S_{3/2} + \hbar\omega)$$

(*b*) ETU

$$Er^{3+}(^4I_{13/2}) + Er(^4I_{13/2}) \rightarrow Er^{3+}(^4I_{9/2}),$$

(*c*) CR

$$Er^{3+}(^4S_{3/2}) + Er(^4I_{15/2}) \rightarrow Er^{3+}(^4I_{9/2}) + Er^{3+}(^4I_{13/2})$$

In this work, we have used Judd-Ofelt theory to calculate the radiative decay rates of the $^4S_{3/2}$, $^4F_{9/2}$, $^4I_{9/2}$, $^4I_{11/2}$, and $^4I_{13/2}$ energy levels and the related luminescence branching ratios of Er^{3+} in tellurite (TZN) glass. In the Judd-Ofelt calculation, the spectroscopic intensity parameters Ω_2, Ω_4, and Ω_6 for Er^{3+}-doped tellurite glass were 5.54×10^{-20}, 1.70×10^{-20}, and 1.22×10^{-20} cm^2, respectively. These values were calculated from absorption measurements made using a CARY spectrophotometer. Values of the angular tensor operator $|\langle U^{(\lambda)} \rangle|^2$ used in the Judd-Ofelt calculation were obtained from the literature[11] for the radiative transitions of Er^{3+} in LaF_3 (aquoions). The refractive index for tellurite (TZNL) glass is n = 1.98 at 1.5 μm.[10]

Figure 1 shows the IR absorption spectra of Er_2O_3(2.2 mol. %)-doped tellurite glass used in this work. The spectrum shows a broad, strong absorption band between 2500 and 3500 cm^{-1}, which is attributed to the free OH^- groups in oxide glasses.[12] In addition, there is a narrow and weak absorption band with maximum at 3735 cm^{-1} that is produced by OH^- isolated impurity. The absorption coefficient (of the OH^- vibration band at 3013 cm^{-1} due to the free OH^- group) is given by $N_{OH} = \frac{N_{Av}\alpha}{\xi}$, where N_{Av} is the Avogadro constant (6.02×10^{23}), α is the absorption coefficient (cm^{-1}), and ξ is the absorptivity of free OH^- groups in the glass. Using $\xi = 49.1 \times 10^3$ cm^2 mol^{-1} (Ref. 13), we estimate the OH^- concentration in our samples as $N_{OH} = 6.25 \times 10^{18}$ cm^{-3} (for $[Er^{3+}] = 2 \times 10^{20}$ cm^{-3}) with $\alpha = 0.51$ cm^{-1}; $N_{OH} = 3.31 \times 10^{18}$ OH^- cm^{-3} (for $[Er^{3+}]$

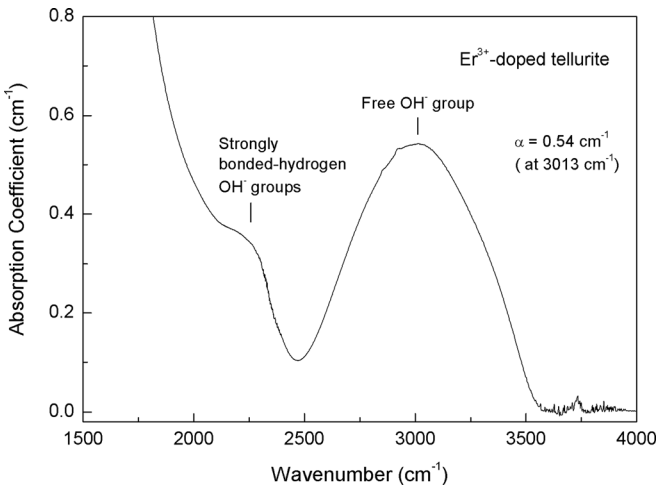

FIG. 1. Measured absorption spectrum of Er_2O_3(2.2 mol. %)-doped tellurite showing the free OH^- group absorption band near 3013 cm^{-1}.

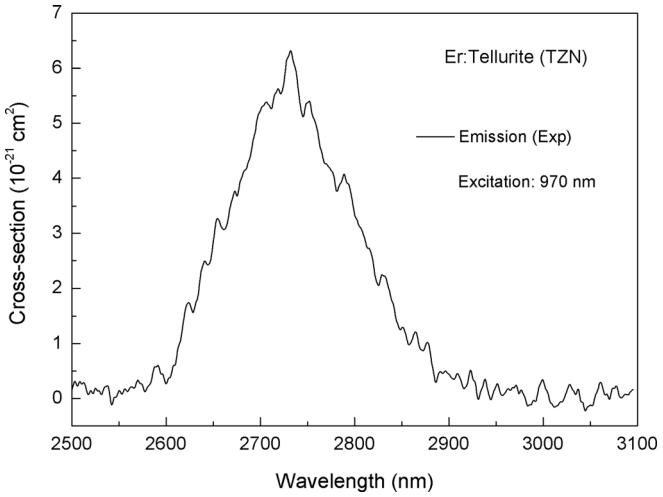

FIG. 2. Measured fluorescence spectrum of the $^4I_{11/2} \rightarrow {}^4I_{13/2}$ transition in Er^{3+}(2.2 mol. %)-doped tellurite glass at T = 300 K. Laser excitation at 971 nm with an average energy of 12 mJ and pulse duration of 4 ns (at 10 Hz).

$= 5 \times 10^{20}$ cm^{-3}) with $\alpha = 0.27$ cm^{-1} and $N_{OH} = 6.61 \times 10^{18}$ cm^{-3} (for $[Er^{3+}] = 1 \times 10^{21}$ cm^{-3}) and $\alpha = 0.54$ cm^{-1}. The highest absorption coefficient corresponding to the $[Er^{3+}] = 2 \times 10^{20}$ cm^{-3} sample, of 0.51 cm^{-1}, is half that measured previously in tellurite glasses melted in a dry atmosphere.[14]

A. Luminescence from the $^4I_{11/2}$ level

Fluorescence emission from the $^4I_{11/2}$ excited state of Er^{3+} was measured for $[Er^{3+}] = 1 \times 10^{21}$ cm^{-3} (or $Er_2O_3 = 2.2$ mol. %), see Fig. 2. The emission cross section was determined after the emission cross section at the fluorescence peak ($\lambda = 2734$ nm) was calculated using the relation $\sigma_{\text{emis}}(\bar{\lambda}) = \frac{\bar{\lambda}^4}{8\pi n^2 c} \frac{2J'+1}{2J+1} \frac{I(\bar{\lambda})}{\int I(\lambda) d\lambda} A_{J,J'}$, where $\bar{\lambda} = 2.734 \times 10^{-4}$ cm, $A_{J,J'} = 34.4$ s^{-1}, $n = 1.98$, $c = 2.998 \times 10^{10}$ cm s^{-1}, and $I(\bar{\lambda}) / \int I(\lambda) d\lambda = 6.407 \times 10^4$ cm^{-1} and J = 11/2 and J' = 13/2. The calculation gave σ_{emis} (2734 nm) $= 4.86 \times 10^{-21}$ cm^2.

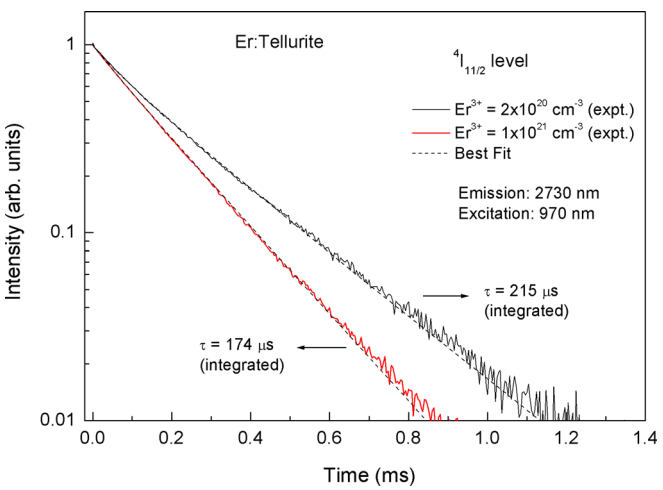

FIG. 3. (Color online) Measured luminescence decay at 2750 nm after pulsed laser (4 ns, 10 Hz) pump at 970 nm (E = 10 mJ) for Er_2O_3(0.5 and 2.2 mol. %)-doped tellurite glass at T = 300 K. The best fit to the measurements using Eq. (1) is represented by the dotted line.

Figure 3 shows the emission decay characteristic at 2750 nm for $[Er_2O_3] = 2.2$ mol. %. It was seen that the luminescence decay of $^4I_{11/2}$ excited state was non exponential and was fitted using Eq. (1) given by Bursthein model,[15] which includes exponential and non-exponential components of the decay.

$$I_1(t) = I_0 \exp\left(-\gamma\sqrt{t} - \frac{t}{\tau_m}\right), \tag{1}$$

where γ is used as a curve fitting parameter to cater for the non-exponential component of the luminescence decay and $\tau_m = \frac{\tau_d}{1+\omega\tau_d}$ is the exponential decay component that accounts for the intrinsic decay rate (radiative decay + non-radiative multiphonon decay) of the donor state, τ_d, and the migration assisted donor to acceptor energy-transfer rate, ω. The mean lifetime is obtained by the integration of the decay curve using Eq. (2). This contains both the exponential and non-exponential components of the fluorescence decay into the one parameter (τ).

$$\tau = \int_0^\infty \exp\left(-\gamma\sqrt{t} - \frac{t}{\tau_m}\right) dt. \tag{2}$$

The best fit of the 2730 nm luminescence was done using Eq. (1) and the fitting parameters were

1) $\gamma = 19.6$ s$^{-1/2}$, $\tau_m = 284.5$ μs, and $\tau = 214.7$ μs for $[Er_2O_3] = 0.5$ mol. %,
2) $\gamma = 9.5$ s$^{-1/2}$, $\tau_m = 231$ μs, and $\tau = 203.7$ μs for $[Er_2O_3] = 1.1$ mol. %, and
3) $\gamma = 8.45$ s$^{-1/2}$, $\tau_m = 193.3$ μs and $\tau = 174.4$ μs for $[Er_2O_3] = 2.2$ mol. %.

We observed that the integrated lifetime value (τ) for the $^4I_{11/2}$ level decreased with $[Er^{3+}]$ increase. This effect was attributed to energy transfer from the $^4I_{11/2}$ level to free OH^- groups that are present in the samples with the estimated concentration of 6.6×10^{18} cm^{-3}. Figure 4(a) shows that the total decay rate (W_{total}) of the $^4I_{11/2}$ level increases with $[Er^{3+}]$ and tends to a constant value for $[Er^{3+}] = 1 \times 10^{21}$ cm^{-3}. This behavior suggests that the critical concentration N_C of Er^{3+} for the $Er^{3+}(^4I_{11/2}) \rightarrow OH^-$ ($\nu = 0 \rightarrow 1$) energy transfer process is reached for an $[Er^{3+}] = 1 \times 10^{21}$ cm^{-3}. As a consequence, the total rate decay of the $^4I_{11/2}$ level (W_{total}) must approximate to a constant value for $[Er^{3+}] > N_C$ [see the experimental data represented by squares in Fig. 4(a)]. Similar behavior has been observed in the interaction between two Er^{3+} ions excited to the $^4I_{11/2}$ level that populate the $^4S_{3/2}$ level by ETU, where the transfer rate has a similar dependence on excited Er^{3+} concentration according to Eq. (3).[13,14]

$$\eta_{OH} = 1 - \exp\left(-\frac{N_{Er}}{N_C}\right) \quad \text{and} \quad W_{total} = \frac{1}{\tau} = C + \eta_{OH} K_0, \tag{3}$$

where η_{OH} is the $Er^{3+} \rightarrow OH^-$ transfer efficiency, τ is the integrated lifetime of the $^4I_{11/2}$ excited state, K_0 is the rate constant parameter for $Er^{3+} \rightarrow OH^-$ transfer, N_{Er} is the Er^{3+} concentration, N_C is the critical concentration of Er^{3+}, and

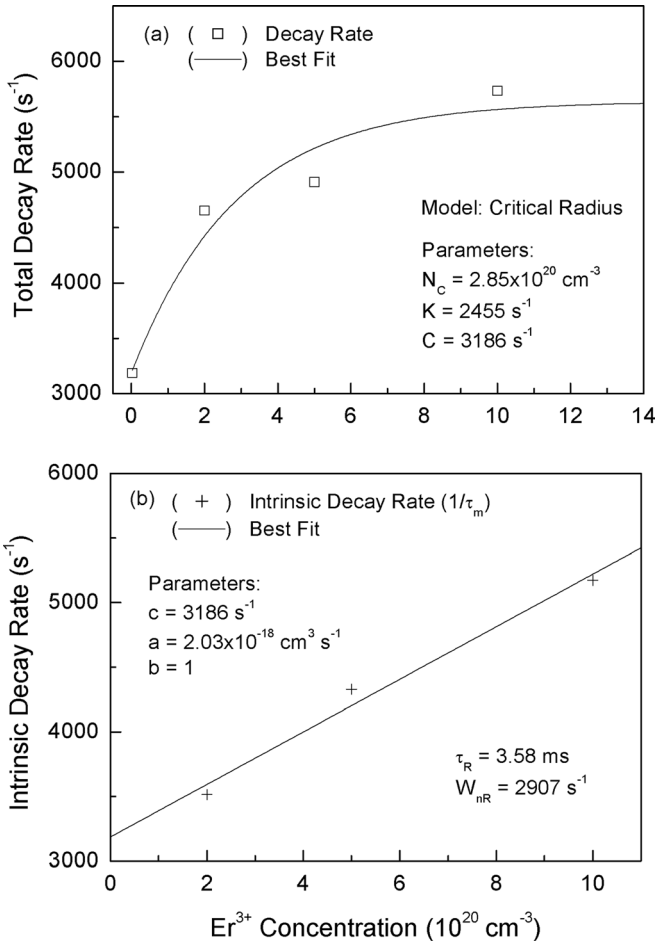

FIG. 4. (a) Measured (total) decay rate (s^{-1}) of the $^4I_{11/2}$ level (open squares) and best fit (solid line) as a function of [Er^{3+}]; (b) shows the measured intrinsic decay rate of the $^4I_{11/2}$ level (crosses) and best fit (solid line) as a function of [Er^{3+}].

C (in s^{-1}) is the intrinsic decay rate of the $^4I_{11/2}$ state, i.e., $C = 1/\tau_R + W_{nR}$. A best fit was carried out by applying the critical radius model, Eq. (3), which gave $N_C = 2.85 \times 10^{20}$ cm^{-3} ($R_C = 9.43$ Å), $C = 3186$ s^{-1}, and $K_0 = 2455$ s^{-1}. Figure 4(b) shows the decay rate due to migration-assisted energy transfer only, i.e., $W_m = 1/\tau_R + W_{nr} + \omega$. The best fit to the data presented in Fig. 4(b) was carried out using the expression $W_m = C + a[Er]^b$ which gave $C = 3186$ s^{-1}, $a = 2.03 \times 10^{-18}$ cm^3 s^{-1}, and $b = 1$. According to this model, $W_{nr} = C - 1/\tau_R$ and using $\tau_R = 2.6$ ms (calculated using Judd-Ofelt theory), one gets $W_{nr} = 2801$ s^{-1}. For the $^4I_{11/2}$ energy level, the OH^- transfer was calculated as the difference between the theoretical decay rate (W_{total}) and the intrinsic decay rate (C). The Er^{3+} ($^4I_{11/2}$) $\rightarrow OH^-$ transfer rates (W_{OH}) were obtained and their values are: 1472 s^{-1} (for [Er_2O_3] = 0.5 mol. %), 1723 s^{-1} (for [Er_2O_3] = 1.1 mol. %), and 2478 s^{-1} (for [Er_2O_3] = 2.2 mol. %). The W_{OH} values are given in Table I. The 2.7 μm luminescence efficiency when pumped into the $^4I_{11/2}$ energy level for each Er^{3+} concentration was calculated to be $\eta_\ell = 0.0826$ for [Er^{3+}] = 2×10^{20} cm^{-3}, $\eta_\ell = 0.0784$ for [Er^{3+}] = 5×10^{20} cm^{-3}, and $\eta_\ell = 0.0680$ for [Er^{3+}] = 1×10^{21} cm^{-3}. Both the multiphonon non-radiative decay and the OH^- energy transfer are the mechanisms responsible for the strong quenching of the decay time of the $^4I_{11/2}$ energy level to 314 μs.

TABLE I. Parameters used in the rate equation modeling for Er-doped tellurite glass.

Luminescence branching ratio and radiative and intrinsic (total) lifetimes of Er^{3+}[a]			
Transition	β (%)	τ_R[b]	τ (expt.)[c] (W_{nr} (s^{-1}))
Er^{3+}:	—	—	—
$^4S_{3/2} \rightarrow$	—	281 μs	53 μs (15462 s^{-1})
$^4F_{9/2}$	0.03	—	—
$^4I_{9/2}$	3.59	—	—
$^4I_{11/2}$	2.21	—	—
$^4I_{13/2}$	27.45	—	—
$^4I_{15/2}$	66.72	—	—
$^4F_{9/2} \rightarrow$	—	300 μs	24 μs (41908 s^{-1})
$^4I_{9/2}$	0.29	—	—
$^4I_{11/2}$	1.68	—	—
$^4I_{13/2}$	4.79	—	—
$^4I_{15/2}$	93.24	—	—
$^4I_{9/2} \rightarrow$	—	2.58 ms	0.83 μs (3.3×10^5 s^{-1})
$^4I_{11/2}$	1.5	—	—
$^4I_{13/2}$	24.8	—	—
$^4I_{15/2}$	73.7	—	—
$^4I_{11/2} \rightarrow$	—	2.60 ms	314 μs (2801 s^{-1})
$^4I_{13/2}$	15.94	—	—
$^4I_{15/2}$	84.06	—	—
$^4I_{13/2} \rightarrow$	—	3.27 ms	3.27 ms (~0 s^{-1})
$^4I_{15/2}$	100	—	—

Energy transfer rate parameters (s^{-1}) (expt.)[d]			
Er_2O_3 (Er^{3+} density (cm^{-3}))	ETU K_0 (s^{-1})	$Er^{3+}(^4I_{11/2}) \rightarrow OH^-$ W_{OH} (3) (s^{-1})	Cross-relaxation W_{CR} (s^{-1})
0.5% (2×10^{20})	383	1472	4234
1.1% (5×10^{20})	1296	1723	14 969
2.2% (1×10^{21})	3782	2478	44 672
(1.2×10^{21})	5046	—	59 243
(1.5×10^{21})	7176	—	83 668

[a]Values obtained from the literature for Er^{3+}(<1%)-doped tellurite.[16]
[b]Radiative lifetimes calculated using Judd-Ofelt theory.
[c]Experimental lifetime (intrinsic) obtained from the best fit to the luminescence.
[d]Experimental transfer rates obtained in this work. The transfer constant given in cm^3 s^{-1} can be obtained using $W = K_0/N_s$, where $N_s = 2 \times 10^{19}$ cm^{-3}.

B. Luminescence decay from the $^4I_{13/2}$ level

Figure 5 shows the measured decay time of the $^4I_{13/2}$ level for two Er_2O_3-doped tellurite samples (0.5 and 2.2 mol. %). The measured decay times for the $^4I_{13/2}$ level are longer than the calculated radiative lifetime ($\tau_R = 3.27$ ms, calculated in this work). The increase in the decay time of the $^4I_{13/2}$ in our experiment relates to strong excitation migration from a resonant dipole-dipole interaction between the $^4I_{13/2}$ and $^4I_{15/2}$ energy levels; this phenomenon explains the initial increase in the decay time as the Er^{3+} concentration was increased. We observed an increase in the decay

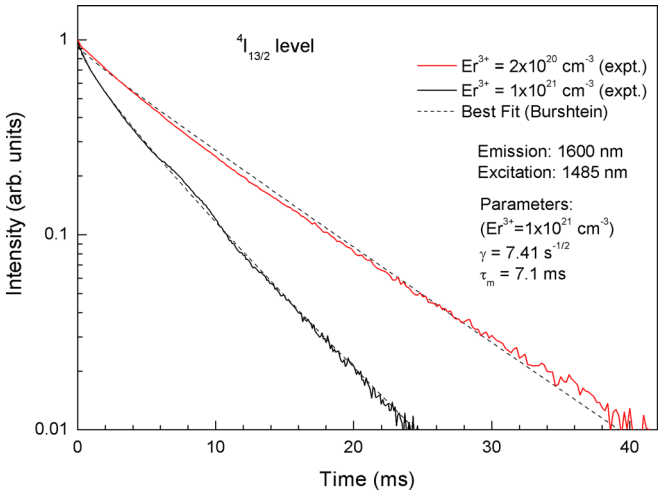

FIG. 5. (Color online) Measured luminescence decay at 1600 nm after pulsed laser (4 ns) pump at 1485 nm for Er_2O_3-doped tellurite T = 300 K (experimental results for $[Er^{3+}] = 0.5$ and 2.2 mol. % only). The best fit to the measurements using Eq. (1) is represented by solid line.

time at distances perpendicular to the pump of ~6 mm, however, for distances of ~3 mm and shorter (from where we took the measurements), the measured decay time was invariable and radiation trapping was constant. The luminescence decay was observed to be non-exponential and a best fit was carried out using Eq. (1) which provided: (1) $\gamma = 3.2$ s$^{-1/2}$ and $\tau_m = 9.6$ ms for $[Er_2O_3] = 0.5$ mol. %, (2) $\gamma = 4.0$ s$^{-1/2}$ and $\tau_m = 12.7$ ms for $[Er_2O_3] = 1.1$ mol. %, and (3) $\gamma = 7.4$ s$^{-1/2}$ and $\tau_m = 7.1$ ms for $[Er_2O_3] = 2.2$ mol. %. Note that the transfer parameter γ increases linearly with $[Er^{3+}]$ concentration, which agrees with Forester-Dexter theory[16] where the donor to acceptor ion transfer parameter, γ, is proportional to the erbium concentration.

An increase in the exponential term, τ_m (whose value is $\tau_m = 9.6$ ms for $[Er^{3+}] = 2 \times 10^{20}$ cm^{-3} and 12.7 ms for $[Er^{3+}] = 5 \times 10^{20}$ cm^{-3}) was observed which indicates strong excitation migration among $^4I_{13/2}$ levels similar to what has been observed for Er^{3+}-doped $LiYF_4$ crystal.[17] In Figure 6, we plot the integrated lifetime τ, (solid squares) and the exponential decay component τ_m (open triangles) for the $^4I_{13/2}$ level as a function of $[Er^{3+}]$. A best fit to the intrinsic lifetime was carried out using Eq. (4); the exponential decay will increase if an Er^{3+} ion excited to the $^4I_{13/2}$ level transfers its energy to a ground state Er^{3+} ion within a critical distance, R_C, with a lifetime augmentation efficiency, $\eta(\tau)$, dependent on $[Er^{3+}]$ (Refs. 17 and 18). This model predicts a saturation of the exponential decay component, τ_m, to a constant value τ_0, which is reached for $N_{Er} > N_C$, where N_C is the critical concentration. The lifetime augmentation efficiency is given by

$$\eta(\tau) = 1 - \exp(-N_{Er}/N_C), \tag{4}$$

where $\tau_m = \tau_R + \eta(\tau)\tau_0$, $\tau_R = 3.27$ ms (calculated using Judd-Ofelt theory), and N_{Er} is the Er^{3+} concentration. The best fit using Eq. (4) gives $\tau_0 = 11.8$ ms and $N_C = 2.8 \times 10^{20}$ cm^{-3} (see red solid line in Fig. 6). The energy transfer rate, W_{OH}, for $Er^{3+}(^4I_{13/2})$ to OH^- ($\nu = 0 \rightarrow 2$) energy transfer process was determined from the difference between the measured decay ($1/\tau$) and the theoretical exponential decay ($1/\tau_m$) calculated using Eq. (4). Using the relation $W_{OH} = 1/\tau - 1/\tau_m$, the following values for W_{OH} were obtained: 16.4 s^{-1} for $[Er_2O_3] = 0.5$ mol. %, 35.6 s^{-1} for $[Er_2O_3] = 1.1$ mol. %, and 164 s^{-1} for $[Er_2O_3] = 2.2$ mol. % were calculated, see Table I.

C. Luminescence from the $^4S_{3/2}$ level

Evidence that the $^4S_{3/2}$ energy level is excited after laser excitation at 970 nm in the Er^{3+}-doped tellurite glass was evident by the observation of green luminescence. The green up-conversion luminescence (see Fig. 7) results from pump ESA from the $^4I_{11/2}$ level because the risetime of the 552 nm luminescence (and hence $^4S_{3/2}$ level population) is ~28 ns, a value close to the response time of the detector (20 ns). If we assume the following pump, two photon absorption (TPA) path: GSA $^4I_{15/2} \rightarrow {}^4I_{11/2}$; ESA1 $^4I_{11/2} \rightarrow {}^4F_{7/2}$ that decays to

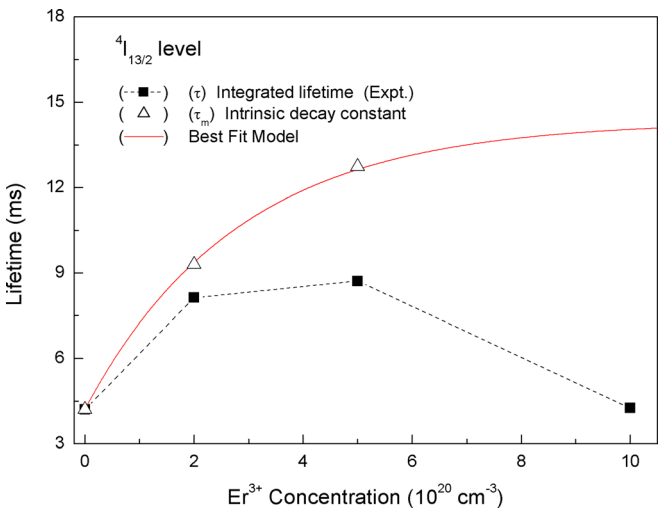

FIG. 6. (Color online) Measured integrated lifetime (solid squares) and intrinsic decay constant (τ_m) (open triangles) of the $^4I_{13/2}$ level as a function of $[Er^{3+}]$. The best fit to the intrinsic decay constant (or exponential term) using Eq. (4) is shown as the red solid line.

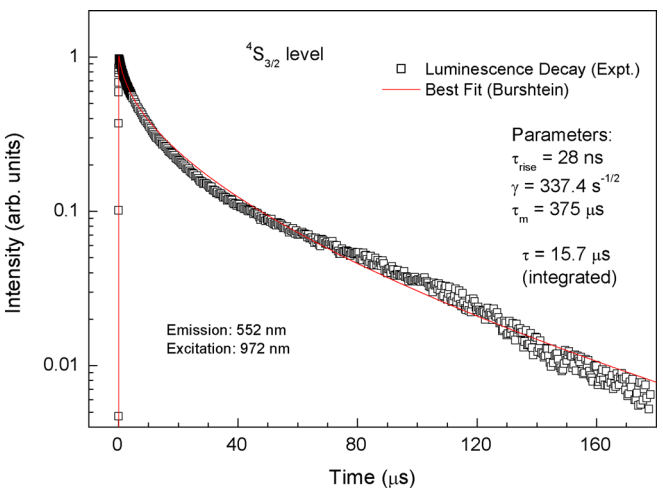

FIG. 7. (Color online) Measured luminescence decay of the $^4S_{3/2}$ level measured at 552 nm for 972 nm laser excitation (pulse energy of 10 mJ and pulse duration of 4 ns) at T = 300 K. The luminescence decay was fitted (solid line) using Eq. (1).

the $^2H_{11/2}$, $^4S_{3/2}$ thermally coupled levels. The best fit to $^4S_{3/2}$ luminescence transient was carried out using the expression $I_2(t) = I_0\left(\exp\left(-\gamma\sqrt{t} - \frac{t}{\tau_m}\right) - \exp\left(-\frac{t}{\tau_{rise}}\right)\right.$, where τ_{rise} is the luminescence risetime and γ and τ_m are the energy transfer parameters due to the cross-relaxation process (process c in Fig. 12) Er^{3+} $(^4S_{3/2}) + Er^{3+}$ $(^4I_{15/2}) \rightarrow Er^{3+}$ $(^4I_{9/2}) + Er^{3+}$ $(^4I_{13/2})$. The decay time (τ) of the $^4S_{3/2}$ level is obtained using Eq. (2). Experimental luminescence data is represented by the squares in Fig. 7 for $[Er^{3+}] = 1 \times 10^{21}$ cm^{-3}, and the solid line represents the curve of best fit, which gives $\tau = 15.7$ μs. The best fit to the 552 nm luminescence was performed using Eq. (1), which gave the following parameters: (1) $\gamma = 50.4$ $s^{-1/2}$, $\tau_m = 59.6$ μs ($R^2 = 0.999$), and $\tau = 43$ μs (integrated) for $[Er^{3+}] = 2 \times 10^{20}$ cm^{-3}; (2) $\gamma = 198$ $s^{-1/2}$, $\tau_m = 158$ μs ($R^2 = 0.991$), and $\tau = 29.4$ μs for $[Er^{3+}] = 5 \times 10^{20}$ cm^{-3} and (3) $\gamma = 337.4$ $s^{-1/2}$, $\tau_m = 375$ μs ($R^2 = 0.997$), and $\tau = 15.7$ μs for $[Er^{3+}] = 1 \times 10^{21}$ cm^{-3}. By plotting the total decay rate ($1/\tau$) of the $^4S_{3/2}$ level as a function of the Er^{3+} concentration, one obtains the intrinsic total decay rate ($1/\tau_d$) of 19021 s^{-1} for the $[Er^{3+}] \rightarrow 0$ where CR is negligible. Using the radiative lifetime $\tau_R = 281$ μs (calculated using Judd-Ofelt theory) in the relation $1/\tau_d = 1/\tau_R + W_{nr}$, one obtains $W_{nr} = 15462$ s^{-1} for the intrinsic non-radiative decay rate of the $^4S_{3/2}$ level. The CR rate was obtained using the relation $W_{CR} = 1/\tau - 1/\tau_d$; see values given in Table I.

Figure 8(a) shows the normalized pump ESA factor, f_{ESA} that was obtained from a best fit to the 552 nm luminescence plotted as a function of the excitation wavelength. It can be observed that the TPA band follows approximately GSA, see Fig. 8(b). By inspection of the minimum and maximum energies of the $^4I_{11/2} \rightarrow {}^4F_{7/2}$ transition of Er^{3+} in tellurite, it can be deduced that the ESA1 spectrum will occur in the range covered by the TPA spectrum. One may obtain the ESA spectrum [or $S(\lambda)$] using the normalized TPA and GSA spectra using

$$S(\lambda) = \frac{TPA(\lambda)}{GSA(\lambda)}. \tag{5}$$

The dashed line in Fig. 8(c) represents the pump ESA spectrum using Eq. (5). Using Judd-Ofelt theory, it is possible to estimate the cross-sections for ESA1. The rate of the strongest radiative transition, $^4F_{7/2} \rightarrow {}^4I_{15/2}$, from $^4F_{7/2}$ excited state was calculated using the reduced matrix elements $U^{(\lambda)}$ for the (Er^{3+} in LaF_3) $U^{(2)} = 0.0$, $U^{(4)} = 0.1467$, and $U^{(6)} = 0.6273$ (Ref. 11) and the corresponding spectroscopic intensity parameters $\Omega_{I=2,4,6}$ (cm^2) given in Sec. III and $\overline{\lambda} = 483$ nm (i.e., the mean emission wavelength). The calculated radiative rate ($A_{i \rightarrow j = 15/2}$) of the $^4F_{7/2} \rightarrow {}^4I_{15/2}$ transition was 6024 s^{-1}. The radiative rate of the $^4F_{7/2} \rightarrow {}^4I_{11/2}$ transition was calculated using relation $A_{(i \rightarrow j=11/2)}/A_{(i \rightarrow j=15/2)} = \frac{\beta_3}{\beta_1}$ and the luminescence branching ratios β_1 (0.86) and β_3 (0.04) for $^4F_{7/2} \rightarrow {}^4I_{15/2}$ and $^4F_{7/2} \rightarrow {}^4I_{11/2}$ transitions, respectively, which are given in Ref. 19. We estimate that $A_{i \rightarrow f(j = 11/2)} = 280$ s^{-1} in Er^{3+}-doped tellurite. The ESA absorption cross section is given by

$$\sigma_{i \rightarrow f}^{abs}(\lambda) = \frac{\overline{\lambda}^4}{8\pi n^2 c} \frac{g_i}{g_f} A_{(i \rightarrow f(j=11/2))} \varepsilon(\lambda), \tag{6}$$

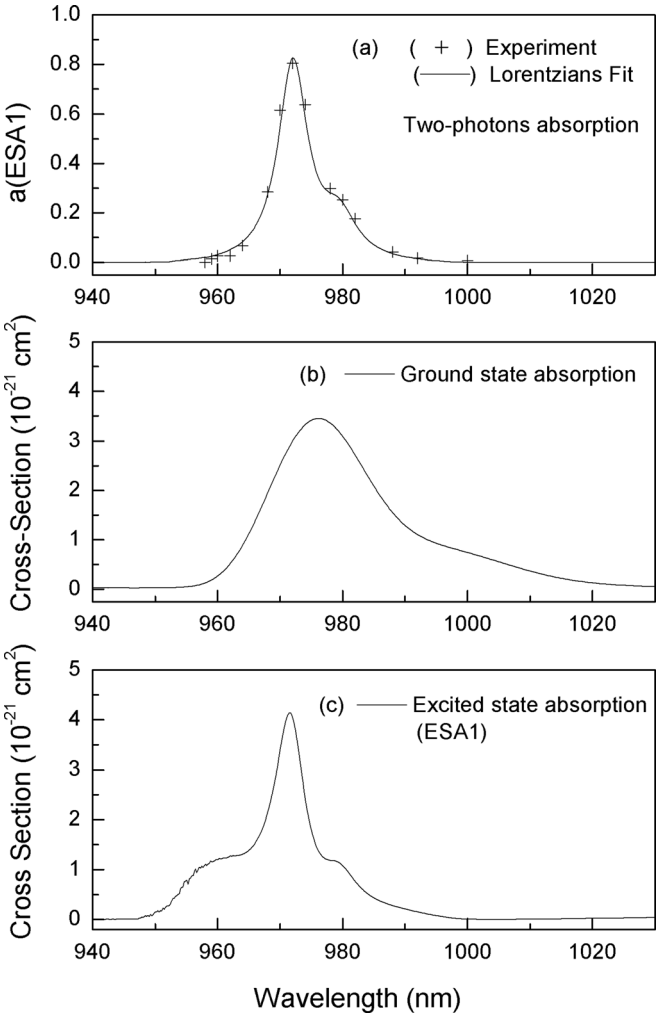

FIG. 8. (a) Measured (crosses) and fitted (two Lorentzian functions, solid line) TPA characteristic given by the $a_{(ESA1)}$ parameter. (b) shows the GSA measured for Er_2O_3 (0.5 mol. %)-doped tellurite and (c) the generated ESA spectrum obtained using Eq. (5) and Eq. (6).

where $\varepsilon(\lambda) = \frac{S(\lambda)}{\int S(\lambda) d\lambda}$ is the line-shape of the ESA spectrum $S(\lambda)$, $g_i = 2J + 1$ and $g_f = 2J' + 1$ (i for the initial and f for the final states), n is the refractive index (1.98), and c the speed of light. The absorption cross-section spectrum due to the $^4I_{11/2} \rightarrow {}^4F_{7/2}$ transition (i.e., ESA1) was calculated using Eq. (6) and $\overline{\lambda} = 971$ nm (average excitation wavelength or centroid), $\varepsilon(\overline{\lambda}) = 0.07313$ nm^{-1}. The cross-section for ESA1 is 4.13×10^{-21} cm^2 at $\overline{\lambda} = 971$ nm. The resultant spectrum for ESA1 was calculated using Eq. (6). Ground state absorption is shown in Fig. 8(b) for comparison.

D. Upconversion to the $^4I_{9/2}$ level

For excitation at ~1485 nm an ETU process Er^{3+} $(^4I_{13/2}) + Er^{3+}$ $(^4I_{13/2}) \rightarrow Er^{3+}$ $(^4I_{15/2}) + Er^{3+}$ $(^4I_{9/2})$ (labeled ETU1) can occur, which populates the $^4I_{9/2}$ level which subsequently emits 810 nm luminescence. By measuring the decay time of the 810 nm luminescence, one can obtain the rate of ETU. Using the "energy-gap" law, expressed as $W_{nr} = C \exp(-\alpha \Delta E)$ for the $^4S_{3/2}$ and $^4I_{11/2}$ levels, the constants $C = 5.97 \times 10^8$ s^{-1} and $\alpha = 3.4 \times 10^{-3}$ cm are obtained

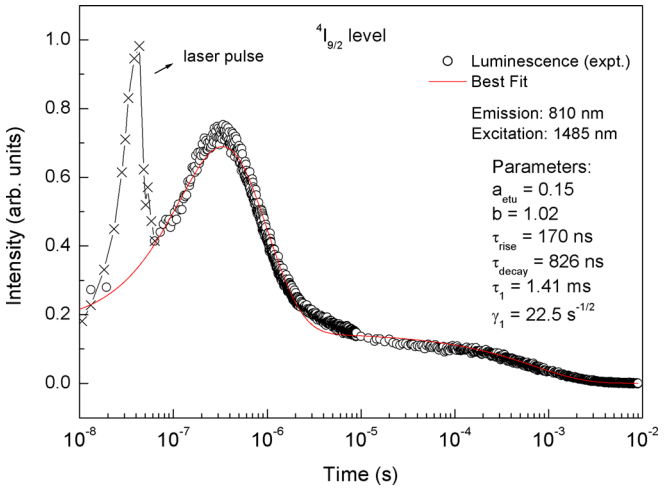

FIG. 9. (Color online) Measured luminescence transient from the $^4I_{9/2}$ level at 810 nm (circles) after laser excitation at 1485 nm (E = 8 mJ) at T = 300 K for Er^{3+}-doped tellurite ($[Er^{3+}] = 1 \times 10^{21}$ cm^{-3}). The excitation pulse (crosses) is also observed. The best fit to the 813 nm luminescence (solid line) was obtained using Eq. (7).

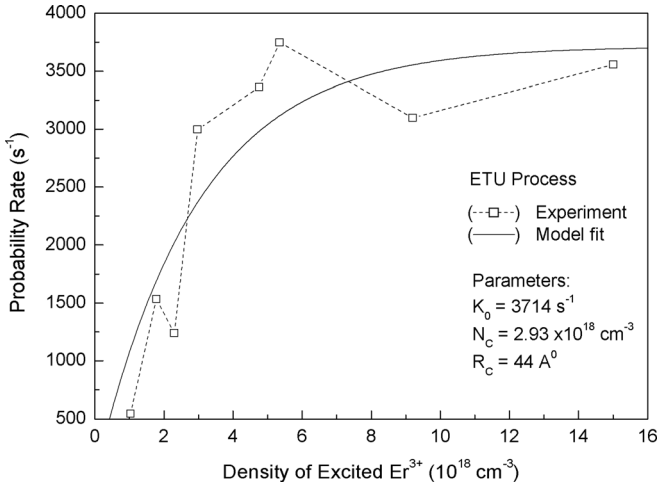

FIG. 10. Measured ETU rate (s^{-1}) as a function of the excited Er^{3+} ion density (N*) obtained by measuring the luminescence transient of the $^4I_{9/2}$ level after pulsed (4 ns) excitation at 1485 nm (squares). The solid line represents the best fit using the critical radius model of Eq. (9). $[Er^{3+}] = 1 \times 10^{21}$ cm^{-3}.

and hence the lifetime of the $^4I_{9/2}$ level was estimated to be 24 μs compared to calculated the radiative lifetime for this level of 2.58 ms.

Figure 9 shows the 810 nm luminescence transient measured after laser pulses (4 ns, E = 10 mJ) at 1485 nm. A short rise time is observed which is then followed by luminescence decay with a time constants of ~1 μs (τ_1) and ~500 μs (τ_2). The values for τ_2 depend on the laser pump intensity and on the Er^{3+} concentration and hence they relate to ETU. The 810 nm luminescence transient was fitted using the following expression:

$$I_3(t) = A\exp(-t/\tau_1) + B\exp(-\gamma_2\sqrt{t} - t/\tau_2) - \exp(-t/\tau_{\text{rise}}), \quad (7)$$

where *(A-B)* gives the amplitude for ESA (labelled $a_{(ESA2)}$) that depends on the excitation wavelength and *B* is related to ETU. The rise time (τ_{rise}) provides the relaxation time from the "*hot excited state*" (or excited $^4I_{9/2}$ level), which will emit one or two-phonons according to the extra excitation energy created by the two-photon excitation (i.e., TPA). The excess energy is ~1088 cm^{-1} for $\lambda = 1485$ nm excitation ($2h\nu = 13\,468$ cm^{-1}) in comparison to the mean energy (12 380 cm^{-1}) for the $^4I_{13/2} \rightarrow {}^4I_{9/2}$ transition. This energy must be dissipated by phonons that will involve a relaxation time (τ_{nr}), which relates to the short rise time, for the $^4I_{9/2}$ luminescence (with a risetime dependent on the excitation wavelength). We obtain: $\tau_{\text{rise}} = 22.5$ ns for $\lambda = 1605$ nm ($\Delta E = 81$ cm^{-1}), $\tau_{\text{rise}} = 160$ ns for $\lambda = 1581$ nm ($\Delta E = 270$ cm^{-1}), $\tau_{\text{rise}} = 170$ ns for $\lambda = 1485$ nm ($\Delta E = 1088$ cm^{-1}), $\tau_{\text{rise}} = 210$ ns for $\lambda = 1476$ nm ($\Delta E = 1170$ cm^{-1}), and $\tau_{\text{rise}} = 260$ ns for $\lambda = 1457$ nm ($\Delta E = 1345$ cm^{-1}). The best fit to the measured luminescence is given by the solid line in Fig. 9 where $A = 1.02$, $B = 0.15$, $\tau_{\text{rise}} = 170$ ns, $\tau_1 = 826$ μs, $\gamma_2 = 22.5$ $s^{-1/2}$, and $\tau_2 = 1.41$ ms ($R^2 = 0.991$) for 1485 nm excitation.

The contribution from ETU was determined using $f_{ETU} = B\int\exp(-\gamma_2\sqrt{t} - t/\tau_2)dt / \int I_3(t)dt$, where $I_3(t)$ is given by Eq. (7). In this case, it was observed that 99% of 810 nm luminescence is produced by ETU (the ESA2 process contributes 1%) for $[Er^{3+}] = 1 \times 10^{21}$ cm^{-3}. Using the fitting parameters γ_2 and τ_2 in Eq. (2), one gets the integrated time constant for ETU (or $\tau_{(ETU)}$), which can be used in Eq. (8) to get the rate of ETU (or $W_{(ETU)}$) where

$$W_{(ETU)} = \frac{1}{\tau_{(ETU)}} - \frac{1}{\tau_d(D)}, \quad (8)$$

and $\tau_d(D)$ is the intrinsic decay time constant of the $^4I_{13/2}$ level [or donor (D)], which in this case $\tau_d(D) = \tau_R = 3.27$ ms.

Figure 10 shows the W_{ETU} values as a function of excited Er^{3+} ions in the $^4I_{13/2}$ level (or laser intensity) for $[Er^{3+}] = 1 \times 10^{21}$ cm^{-3} when pumped at 1485 nm. It can observed that the rate of ETU increases with the excitation density (N^*), which tends to saturate for $N^* \sim 2 \times 10^{19}$ cm^{-3} similarly to observations made of the $^4I_{13/2}$ level in Er^{3+}(15 mol. %)-doped $LiYF_4$ crystal.[17] This means that the critical radius model can be applied to describe how the rate of ETU depends on the excitation density (N^*). This model is given by[17,18]

$$\eta_{ETU} = 1 - \exp(-N^*/N_C), \quad (9)$$

where N^* is the $^4I_{13/2}$ level and N_C is the critical concentration of Er^{3+} ions excited to the $^4I_{13/2}$ ions given by $N_C = \left((4\pi/3)R_C^3\right)^{-1}$. The fact that W_{ETU} approaches a constant value for a high excitation density (N_S), see Fig. 10 indicates that the efficiency for ETU at large values of N^* should be given by $\eta_{ETU}(N^*) = W_{ETU}/K_0$, where K_0 is the rate constant parameter. The solid line in Fig. 10 represents the best fit for W_{ETU} using the critical radius model for $[Er^{3+}] = 1 \times 10^{21}$ cm^{-3} where $N_C = 2.93 \times 10^{18}$ cm^{-3} (or $R_C = 44$ Å) and $K_0 = 3782$ s^{-1}. It can be observed that W_{ETU} approaches the K_0 value when $N_S = 2 \times 10^{19}$ cm^{-3}, which gives $W_{ETU}^{cte} = 1.89 \times 10^{-16}\,cm^3s^{-1}$, where $W_{ETU}^{cte} = K_0/N_S$. This value for W_{ETU} for $Er_2O_3 = 2.2$ mol. % is about 3 times larger than the equivalent rate for Er^{3+}(15 mol. %)-doped $LiYF_4$ crystal.[17] The rate constants for ETU are presented in Table I.

The strength of pump ESA from the $^4I_{13/2}$ level (labeled ESA2) and its wavelength dependence is given by the amplitude (*A*-*B*) [labeled the $a_{(ESA2)}$ parameter in Eq. (7)] and was obtained for many excitation wavelengths across the $^4I_{15/2} \rightarrow {}^4I_{13/2}$ absorption spectrum i.e., 1450 nm to 1650 nm. Fig. 11(a) shows the pump ESA factor, $a_{(ESA2)}$ obtained from a best fit to the 810 nm luminescence plotted as a function of the excitation wavelength. It can be observed that the TPA band follows approximately with GSA, see Fig. 11(b). By inspection of the minimum and maximum energies of the $^4I_{13/2} \rightarrow {}^4I_{9/2}$ transition of Er^{3+} in tellurite, it can be deduced that the ESA1 spectrum will occur in the range covered by the TPA spectrum with an excess average excitation energy of $\sim$570 cm^{-1}. It means that one phonon of energy 570 cm^{-1} must be emitted (or created) following TPA. Note that the phonon energy created in this process has a lower energy than the phonons (with energy $\sim$705 cm^{-1}) involved in multiphonon nonradiative decay.

The one-phonon sideband ESA spectrum [or SB(λ)] can be obtained using the normalized TPA and GSA spectra using Eq. (5); see the solid curve of Fig. 11(c), however, one can extract the ESA spectrum [or S(λ_1^+)] due to the $^4I_{13/2} \rightarrow {}^4I_{9/2}$ transition (centered at 1700 nm) by shifting the wavelength λ to λ_1^+ according to the relation $\lambda_1^+ = (1/\lambda - \hbar\omega)^{-1}$, where $\hbar = 570\ cm^{-1}$ is the mean energy absorbed by the lattice.[20] The sideband amplitude must be scaled using the one-phonon creation probability P_1^+ that is given by $P_1^+ \cong S_0(\overline{n}+1)\exp(-(2\overline{n}+1)S_0)$, where $\overline{n} = [\exp(\hbar\omega/KT) - 1]^{-1}$ is the occupation number of the phonon mode (at T = 300 K). $S_0 \sim 0.31$ is the electron-phonon coupling (or Huang-Rhys factor) and $\hbar = 570\ cm^{-1}$ is the average phonon energy of all the phonon modes which couples to the multiphonon sideband absorption relevant to tellurite glass. The ESA spectrum was obtained according to the relation: $S(\lambda_1^+) = P_1^+ SB(\lambda \rightarrow \lambda_1^+)$, where $P_1{}^+ = 0.2324$. The dashed line in Fig. 11(c) shows the ESA2 spectrum centered at 1700 nm and the solid line in Fig. 11(c) shows the pump ESA spectrum using Eq. (5).

We can estimate the cross-section for ESA2 using Eq. (6), where $\overline{\lambda} = 1700$ nm (mean absorption wavelength), $n = 1.98$, and $A^{ed}_{i\rightarrow j=13/2} = 89\ s^{-1}$ (calculated in this work for the $^4I_{9/2} \rightarrow {}^4I_{13/2}$ transition). Using the measured line-shape of ESA2 spectrum, $\varepsilon(\overline{\lambda}) = 0.00438\ nm^{-1}$, we have $\sigma(\text{ESA2}) = 7.88 \times 10^{-22}\ cm^2$ at $\overline{\lambda} = 1700$ nm. The one-phonon sideband ESA2 cross-section at $\overline{\lambda} = 1550$ nm was obtained using the relation $\sigma^{ESA2}_{one-phonon} = P_1^+ \sigma(ESA2)$, where $P_1^+ = 0.2324$, which gives a cross-section of 1.83×10^{-22} cm^2 at 1550 nm.

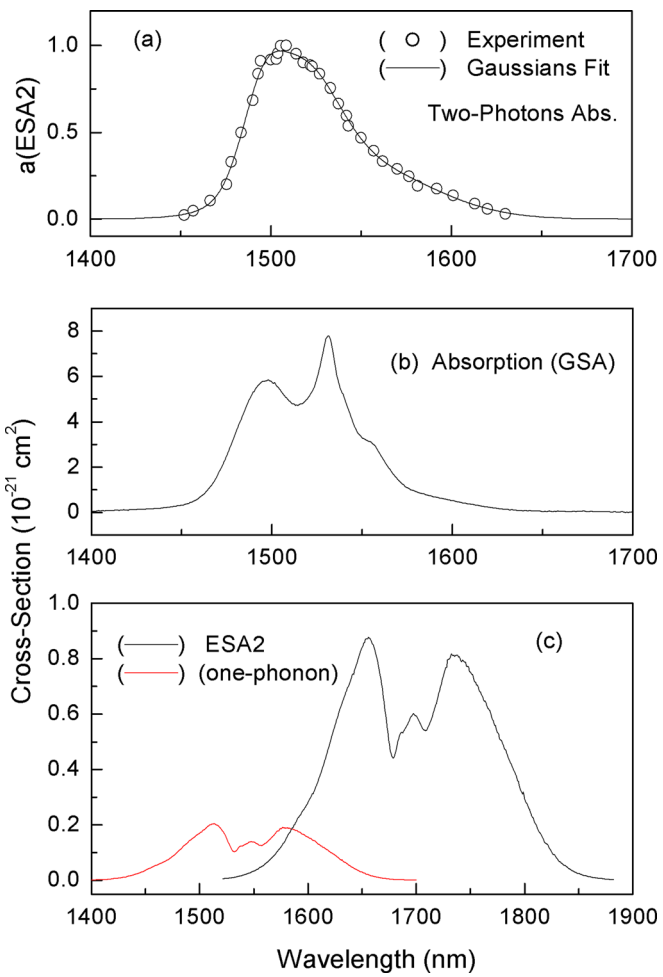

FIG. 11. (Color online) (a) Measured emission at 813 nm (circles) from the $^4I_{9/2}$ level after pulsed laser excitation across the $^4I_{15/2} \rightarrow {}^4I_{13/2}$ GSA transition. The solid line is the best fit using two Gaussian functions, (b) measured GSA spectrum, and (c) calculated ESA spectrum and side-band ESA spectrum for $[Er^{3+}] = 1 \times 10^{21}\ cm^{-3}$.

IV. DISCUSSION

In an effort to predict the performance of fibre lasers operating on the 3 μm transition, we carried out numerical modeling of the system using the spectroscopic parameters determined above. Figure 12 shows the simplified energy level scheme of the Er^{3+}-doped tellurite system for cw pumping at 976 nm. n_1, n_2, n_3, n_4, and n_5 represent the $^4I_{15/2}$, $^4I_{13/2}$, $^4I_{11/2}$, $^4F_{9/2}$, and $^4S_{3/2}$ level populations most relevant to the laser transition at 2.75 μm. The $^4F_{7/2}$ and $^2H_{11/2}$ excited levels were not considered because they are strongly depopulated by fast multiphonon decay to the $^4S_{3/2}$ level. (Similarly, the $^4I_{9/2}$ decays quickly to the $^3I_{11/2}$ level.) The rate equations for our model using the normalized population $n_1 + n_2 + n_3 + n_4 + n_5 = 1$ are

$$\frac{dn_1}{dt} = -R_P n_1 + \frac{n_2}{\tau_{R2}} + \frac{\beta_{51}}{\tau_{R5}} n_5 + \frac{\beta_{41}}{\tau_{R4}} n_4 + \frac{\beta_{31}}{\tau_{R3}} n_3 + K n_2^2 - W_{CR} n_1 n_5 + W_{OH}(2) n_2, \quad (10)$$

$$\frac{dn_2}{dt} = -\frac{n_2}{\tau_{R2}} + \frac{\beta_{52}}{\tau_{R5}} n_5 + \frac{\beta_{42}}{\tau_{R4}} n_4 + \frac{\beta_{32}}{\tau_{R3}} n_3 + W_{nR}(32) n_3 - 2K n_2^2 + W_{CR} n_1 n_5 - W_{OH}(2) n_2 + W_{OH}(3) n_3, \quad (11)$$

$$\frac{dn_3}{dt} = R_P n_1 - R_{ESA1} n_3 - \frac{n_3}{\tau_{R3}} - W_{nR}(32) n_3 + \frac{\beta_{53}}{\tau_{R5}} n_5 + \frac{\beta_{43}}{\tau_{R4}} n_4 + W_{nR}(43') n_4 + K n_2^2 + W_{CR} n_1 n_5 - W_{OH}(3) n_3, \quad (12)$$

$$\frac{dn_4}{dt} = -\frac{n_4}{\tau_{R4}} - W_{nR}(43') n_4 + \frac{\beta_{54}}{\tau_{R5}} n_5 + W_{nR}(54) n_5, \quad (13)$$

$$\frac{dn_5}{dt} = R_{ESA1} n_3 - \frac{n_5}{\tau_{R5}} - W_{nR}(54) n_5 - W_{CR} n_1 n_5, \quad (14)$$

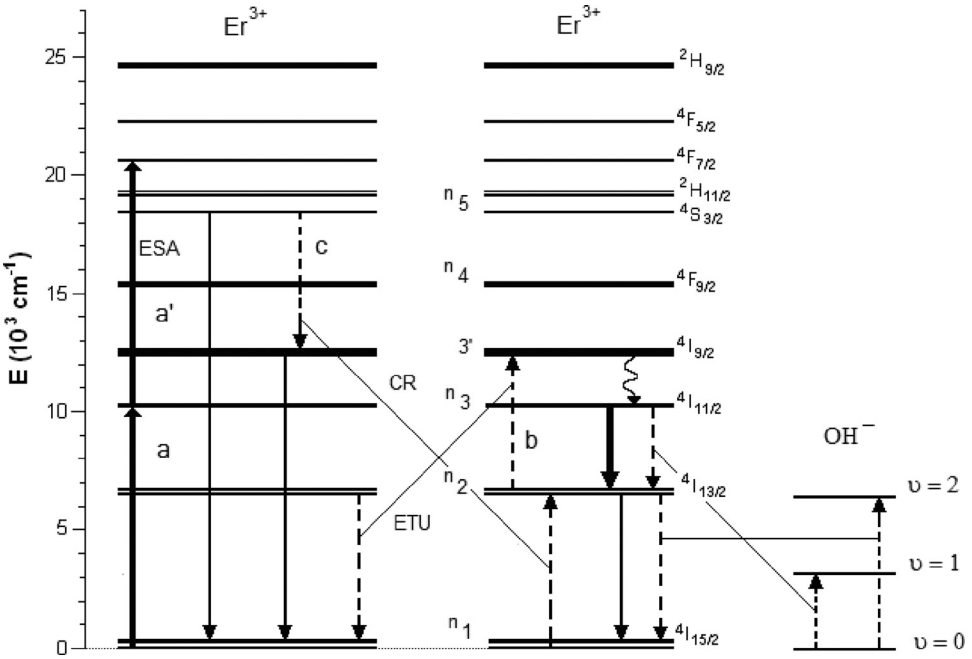

FIG. 12. Simplified energy level scheme for Er^{3+}-doped tellurite glass showing the energy transfer process relevant to laser operation at 2750 nm.

where $R_P = \sigma_{13}\frac{I_P}{h\nu_P}$ is the pump rate (s^{-1}), I_P is the pump light (W cm^{-2}), and $h\nu_P$ is the photon energy of pump radiation. β_{ij} represents the luminescence branching ratio and τ_{Ri} is the radiative lifetime. The fundamental and excited state absorption cross-sections are $\sigma_{13} = 3.45 \times 10^{-21}$ cm^2 (GSA) and $\sigma_{35} = 1.39 \times 10^{-21}$ cm^2 at 976 nm (ESA1). The emission cross-section, $\sigma_{32} = 6.29 \times 10^{-21}$ cm^2 (at $\lambda = 2734$ nm). Experimental values of the intrinsic total decay times (τ_2, τ_3, and τ_5), radiative lifetimes (τ_{Ri}), luminescence branching ratios (β_{ij}), multiphonon decay rates ($W_{nR}(32)$, $W_{nR}(43')$, $W_{nR}(54)$), and W_{OH} (i) where $i = 2$, 3 for the Er^{3+} concentrations used in this work are given in Table I.

The calculated evolution of the excited state populations (in cm^{-3}) obtained by numerical simulation of the rate equations for $[Er^{3+}] = 1.5 \times 10^{21}$ cm^{-3} using a pumping rate of 1000 s^{-1} (or $I_P = 59.3$ kW cm^{-2}) is shown in Fig. 13(a), where one can observe that equilibrium occurs for a time shorter than 3 ms. At equilibrium, the populations n_3 and n_2 were taken and the population inversion $\Delta n = n_3 - n_2$ was obtained for $[Er^{3+}] = 1 \times 10^{21}$ cm^{-3}, 1.2×10^{21} cm^{-3}, and 1.5×10^{21} cm^{-3} as a function of the pump intensity at 976 nm; these results are presented in Fig. 13(b), which indicates a threshold pump intensity that depends on the Er^{3+} concentration [I_P *(threshold)* ~87 kW cm^{-2} for $Er^{3+} = 1.2 \times 10^{21}$ cm^{-3}] if we assume that $W_{OH}(2) = W_{OH}(3) = 0$, i.e., a glass without OH^- impurity. We calculate a negative population inversion for $[Er^{3+}] = 1.5 \times 10^{21}$ cm^{-3} if we include $Er^{3+}(^4I_{11/2}) \rightarrow OH^-$ energy transfer with $[OH^-] = 6.6 \times 10^{18}$ cm^{-3}. Overall, we calculate that Er^{3+}-doped tellurite will not have gain at 2.75 μm unless $[Er^{3+}]$ is at least 1.2×10^{21} cm^{-3} which provides an ETU rate (K_1) of $1.7124 \times W_{nr}(32)$. In this case, a positive population inversion occurs when the threshold pumping intensity of ~87 kW cm^2 is attained.

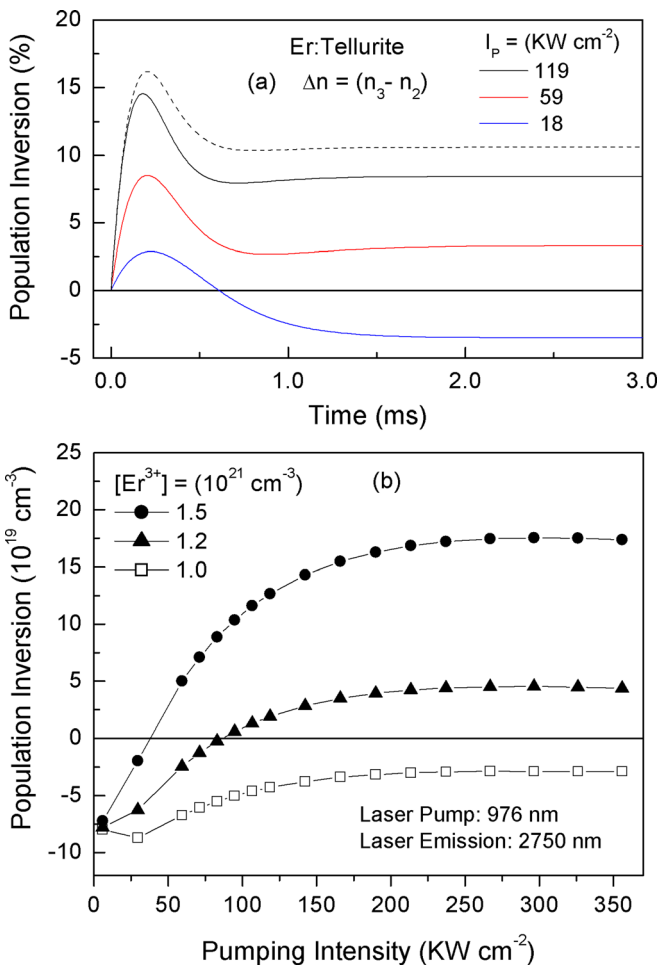

FIG. 13. (Color online) (a) Calculated population inversion for $[Er^{3+}] = 1.5 \times 10^{21}$ cm^{-3} in tellurite glass for cw pumping at 976 nm for varying pumping intensities. ESA1 was switched off (dashed line) to show its contribution ($I_P = 119$ KW cm^{-2}). (b) Calculated population inversion as a function of the pump rate for $[Er^{3+}] = 1 \times 10^{21}$, 1.2×10^{21}, and 1.5×10^{21} cm^{-3}.

V. CONCLUSIONS

The intrinsic luminescence efficiency of the $^4I_{11/2} \rightarrow {}^4I_{13/2}$ transition of Er^{3+}-doped tellurite glass at $T = 300\,K$ was determined to be 0.83%; a value primarily the result of large rates of multiphonon emission. We have observed that the decay time of the $^4I_{11/2}$ and $^4I_{13/2}$ levels in our samples was Er^{3+} concentration dependent, which we attribute to migration-assisted energy transfer to OH^- radicals present in the glass. The transfer rate from Er^{3+} ($^4I_{11/2}$) to OH^- radicals (at a measured concentration of 6.6×10^{18} cm^{-3}) is ~85% of the multiphonon decay rate for $[Er^{3+}] = 1 \times 10^{21}$ cm^{-3} and consequently reduces further the luminescence efficiency to 0.046%. We measured ETU between excited Er^{3+} ions in the $^4I_{13/2}$ level with a rate increasing with the Er^{3+} concentration; we established that this process is essential for the creation of the population inversion on the laser transition at 2.75 μm, however, the ETU rate constant of 3714 s^{-1} measured for $[Er^{3+}] = 1 \times 10^{21}$ cm^{-3} was not enough to create a population inversion in tellurite glass, even for the ideal case where $[OH^-] = 0$. For $[Er^{3+}] >= 1.2 \times 10^{21}$ cm^{-3} (or Er_2O_3 ~2.65 mol. %) and $[OH^-] = 0$, a population inversion was determined for a threshold pumping intensity of ~87 kW cm^{-2} at 976 nm. It was established that pump ESA processes at 976 nm would have a detrimental impact on the performance of Er^{3+}-doped tellurite fibre laser performance.

ACKNOWLEDGMENTS

The authors thank financial support from FAPESP (Grants Nos. 1995/4166-0 and 2000/10986-0), CNPq, and the Australian Research Council.

[1]S. R. Bowman, IEEE J. Quantum Electron. **32**, 646 (1996).
[2]M. C. Nostrand, R. H. Page, S. A. Payne, L. I. Isaenko, and A. P. Yelisseyev, J. Opt. Soc. Am. B 1**8**, 264 (2001).
[3]T. Schweizer, D. W. Hewak, B. N. Samson, and D. N. Payne, Opt. Lett. **21**, 1594 (1996).
[4]S. D. Jackson, Appl. Phys. Lett. **88**, 221106 (2006).
[5]S. D. Jackson, T. A. King, and M. Pollnau, Opt. Lett. **24**, 1133 (1999).
[6]X. S. Zhu and R. Jain, Opt. Lett. **32**, 26 (2007).
[7]S. Tokita, M. Murakami, S. Shimizu, M. Hashida, and S. Sakabe, Opt. Lett. **34**, 3062 (2009).
[8]D. Faucher, M. Bernier, G. Androz, N. Caron, and R. Vallee, Opt. Lett. **36**, 1104 (2011).
[9]J. Wang, E. Vogel, and E. Snitzer, Opt.Mat. **3**, 187 (1994).
[10]M. R. Oermann, H. Ebendorff-Heidepriem, Y. H. Li, T. C. Foo, and T. M. Monro, Opt. Express **17**, 15578 (2009).
[11]M. J. Weber, Phys. Rev. **157**(2), 157 (1967).
[12]M. Arnaudov, Y. Dimitriev, V. Dimitrov, and M. Dimitrovapank, Phys. Chem. Glasses **27**, 48 (1986).
[13]H. Gebavi, D. Milanese, G. Liao, Q. Chen, M. Ferraris, M. Ivanda, O. Gamulin, and S. Taccheo, J. Non-Crystal. Solids **355**, 548 (2009).
[14]L. Nemec and J. Gotz, J. Am. Ceram. Soc. **53**, 526 (1970).
[15]X. Feng, S. Tanabe, and T. Hanada, J. Non-Cryst. Solids **281**, 48 (2001).
[16]A. I. Burshtein, JETP Lett. **35**, 882 (1972).
[17]L. Gomes, A. F. H. Librantz, F. H. Jagosich, W. A. L. Alves, I. M. Ranieri, and S. L. Baldochi, J. Appl. Phys. **106**, 103508 (2009).
[18]A. F. H. Librantz, S. D. Jackson, F. H. Jagosich, L. Gomes, G. Poirier, S. J. L. Ribeiro, and Y. Messaddeq, J. Appl. Phys. **101**, 123111 (2007).
[19]C. Li, Y. Guyot, C. Linarés, R. Moncorgé, and M. F. Joubert, "Radiative Transition Probabilities of Trivalent Rare-Earth Ions in $LiYF_4$," in *Advanced Solid State Lasers*, A. Pinto and T. Fan, eds., OSA Proceedings Series (Optical Society of America, 1993), paper NL7.
[20]L. V. G. Tarelho, L. Gomes, and I. M. Ranieri, Phys. Rev. B **56**, 14344 (1997).